Quaternary Research 84 (2015) 335–347

Contents lists available at ScienceDirect

Quaternary Research

journal homepage: www.elsevier.com/locate/yqres

Paleohydrology of the Santiaguillo Basin (Mexico) since late last glacial and climate variation in southern part of western subtropical North America

Priyadarsi D. Roy [a,*], Claudia M. Chávez-Lara [b], Laura E. Beramendi-Orosco [a], José L. Sánchez-Zavala [a], Gowrappan Muthu-Sankar [c], Rufino Lozano-Santacruz [a], Jesús D. Quiroz-Jimenez [b], Nayeli López-Balbiaux [d]

[a] Instituto de Geología, Universidad Nacional Autónoma de México, 04510 México DF, Mexico
[b] Posgrado en Ciencias de la Tierra, Universidad Nacional Autónoma de México, 04510 México DF, Mexico
[c] French Institute of Pondicherry, 11, St. Louis Street, Pondicherry 605001, India
[d] USAI, Facultad de Química, Universidad Nacional Autónoma de México, 04510 México DF, Mexico

ARTICLE INFO

Article history:
Received 1 December 2014
Available online 6 November 2015

Keywords:
Paleoclimate
Geochemistry
Late last glacial–Holocene
Subtropical North America
Tropical Cyclone
North American Monsoon
Mexico

ABSTRACT

Stratigraphy, geochemistry and radiocarbon dating of a succession of sediment in the Santiaguillo Basin (central-northern Mexico) help reconstruct the millennial-scale dynamics of hydrological variability that occurred in the southern part of western subtropical North America since the late last glacial. Runoff was generally above average during the late last glacial from ~27 to 18 ka. Following this interval, runoff decreased and deposition of authigenic carbonate and aeolian transported sediment increased until ~4 ka. Heinrich 1 and 2, and Younger Dryas were intervals of reduced runoff and increased aeolian activity. The wetter climate of central-northern Mexico and arid conditions in north–northwestern Mexico during the late last glacial were probably related to formation of tropical cyclones in the eastern North Pacific during the autumn with restricted rainfall swaths and an absent/weaker North American Monsoon. Enhanced North American Monsoon and tropical cyclones with expanded rainfall swaths brought more summer and autumn precipitation to a broader region extending from the central-northern Mexico to the continental interiors of southwestern US during the early Holocene.

Introduction

Modern day climate of the subtropical North America is controlled by summer and autumn rainfalls associated with the North American Monsoon (NAM) and tropical cyclones (Douglas et al., 1993; Stensrud et al., 1995; Higgins et al., 1997; Mitchell et al., 2002; Amador et al., 2006; Farfán and Fogel, 2007; Ritchie et al., 2011) as well as winter precipitation related to the westerly jet stream (Friedman et al., 1992; Cayan et al., 2008; Caldwell, 2010; Neelin et al., 2013). The Pacific coast of the southwestern US is dominated by winter precipitation (Friedman et al., 1992; Cayan et al., 2008; Caldwell, 2010; Neelin et al., 2013), whereas northern and northwestern Mexico are dominated by summer and autumn precipitation (Douglas et al., 1993; Stensrud et al., 1995; Mitchell et al., 2002; Xu et al., 2004; Farfán and Fogel, 2007). The continental interiors of southwestern US receive summer and autumn precipitation as well as winter rainfall (Sheppard et al., 2002). Figure 1 shows the present precipitation regimes from different sites (www.weatherbase.com) and divides the region into northern, central and southern parts based on locations of the comparison sites.

Numerous researchers suggest that more winter storms provided greater precipitation to the region during the global last glacial maximum (LGM) in western subtropical North America (COHMAP members, 1988; Thompson and Anderson, 2000; Enzel et al., 2003). COHMAP members (1988) and Kutzbach and Wright (1985) suggested that the Laurentide ice sheet split the jet streams into two different branches and the stronger southern branch carried more moisture into the region. However, the global climate simulations of Kim et al. (2008) and Toracinta et al. (2004) either did not support the split in the jet stream or indicated that the southern branch of the jet stream was weaker. The high-resolution model of Kim et al. (2008) locates the region of dominant winter precipitation in the western–southwestern US and region of dominant summer precipitation in northwestern Mexico. This model's simulation also shows that summer precipitation was occurring in the continental interiors of southwestern US. The juxtaposition of cold ice sheet and adjacent warm ice-free land caused a pronounced low-level thermal gradient and facilitated the development of synoptic cyclones at the southern margin of Laurentide ice sheet (Bromwich et al., 2005). Recently, Oster et al. (2015) compared a compilation of proxy precipitation reconstructions from the region with climate simulations and suggested that the hydroclimate of LGM is best explained by a stronger jet stream that is squeezed and steered across the continent.

* Corresponding author.
E-mail addresses: priyadarsi1977@gmail.com, roy@geologia.unam.mx (P.D. Roy).

http://dx.doi.org/10.1016/j.yqres.2015.10.002
0033-5894/

https://doi.org/10.1016/j.yqres.2015.10.002 Published online by Cambridge University Press

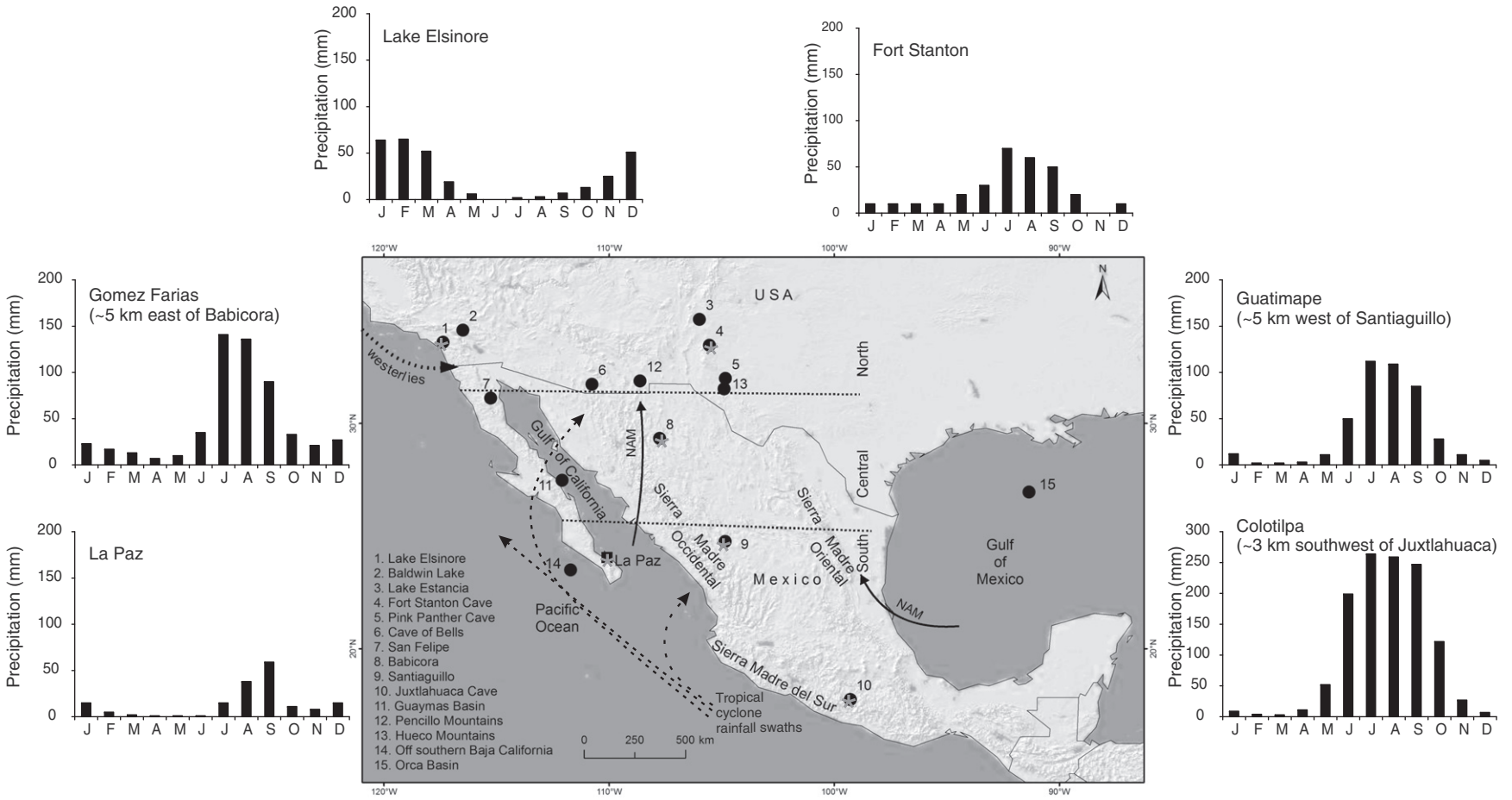

Figure 1. Location of paleoclimate archives (filled circle) from the western subtropical North America. The Santiaguillo Basin is located at ~ 25°N in the eastern flank of Sierra Madre Occidental Mountains in central-northern Mexico. Modern precipitation data from different sites (star) of the region are shown (source: www.weatherbase.com).

Over the last two decades, the number of proxy-records from the region has increased thus improving the knowledge of LGM climate across the southwestern US and northwestern Mexico (Anderson et al., 2002; Holmgren et al., 2003, 2007; Kirby et al., 2005, 2006, 2013; Asmerom et al., 2010; Roy et al., 2010, 2012, 2013; Wagner et al., 2010; Lachniet et al., 2014) (Fig. 1). More winter precipitation in the southwestern US is reflected by the presence of permanent lakes in coastal southern California, negative excursions in $\delta^{18}O$ values of speleothems from Nevada, Arizona and New Mexico and absence of summer flowering annuals and C_4 grasses in the US and Mexico borderland (Kirby et al., 2005, 2006; Holmgren et al., 2007; Asmerom et al., 2010; Wagner et al., 2010). At the same time, the lacustrine basins from Baja California and Chihuahua received less runoff as a result of reduced summer precipitation in northern and northwestern Mexico (Roy et al., 2010, 2012).

Over the deglaciation, the amount of summer precipitation increased in northern and northwestern Mexico (Roy et al., 2010, 2012). Lyle et al. (2012) suggested that the northward expansion of summer precipitation brought humid air mass into the Great Basin in the interior of the western US. However, Kirby et al. (2013) and Lachniet et al. (2014) did not recognize any evidence of summer rainfall reaching the coastal southern California and central Great Basin and suggested that variations in the hydrological conditions of Lake Elsinore and Leviathan Cave were controlled by different amounts of winter precipitation. During the Pleistocene–Holocene transition, an interval of alluvial fan aggradation in the southwestern US is explained by the enhanced frequency of winter storms as well as increased penetration of tropical cyclones (Antinao and McDonald, 2013). In a regional synthesis of Holocene records, Metcalfe et al. (2015) re-analyzed the influences of both summer and autumn insolation and latitudinal migration of Inter-Tropical Convergence Zone (ITCZ) on climate signals of the NAM region. Barron et al. (2012) reported presence of enhanced moisture in a broader NAM region during the early Holocene (>8 ka; all ages in this paper are presented as calendar years before AD 1950) and related it to the moisture flow sourced from the subtropical Pacific compared to the regular Gulf of California (GoC).

Paleoclimatic details for central-northern Mexico come from our previous work in the Santiaguillo Basin (Roy et al., 2014). An enhancement in the amount of runoff into the Santiaguillo Basin during the Pleistocene–Holocene transition and early Holocene was associated with more monsoonal moisture sourced from GoC. In this study, we present new geochemical (organic carbon, carbonate, C/N, and elemental concentrations) and magnetic susceptibility data extending our knowledge about runoff, evaporation and lake salinity, provenance of organic productivity and clastic sediments in the basin, and aeolian activity up to 27 ka. The paleohydrological information is compared with our recently published register of paleoecology of ostracods from the same sediment profile (Chávez-Lara et al., 2015). The runoff record for the Santiaguillo Basin is compared with proxy records from the Juxtlahuaca Cave (southwestern Mexico; Lachniet et al., 2013) and Lake Elsinore (coastal southwestern US; Kirby et al., 2013). Both the Juxtlahuaca Cave (monsoonal only) and Lake Elsinore (winter only) are end member sites and the comparison enables us to estimate the influences of monsoonal and winter precipitations on the hydrological variations in the Santiaguillo Basin. We evaluated the influences of different forcings on the Santiaguillo Basin record through comparison to insolation values (Berger and Loutre, 1991), reconstructed North Hemisphere temperature (NGRIP project members, 2004), mean position of ITCZ (Deplazes et al., 2013), sea surface temperature (SST) records from GoC (McClymont et al., 2012) and Gulf of Mexico (GoM; Flower et al., 2004), and contemporary meteorological data about the NAM and tropical cyclones.

Material and methods

Study site

The ephemeral and endorheic Santiaguillo Basin is located in a half-graben in central-northern Mexico (24° 44′ N, 104° 48′ W, 1960 m asl) along the eastern flank of Sierra Madre Occidental Mountains (Fig. 1). The half-graben was formed at ~ 39–32 Ma (Nieto-Samaniego et al., 2012) and the present lacustrine basin is spread over an area of ~ 2000 km^2. The basin is oriented NW–SE, and has a maximum length and width of ~ 45 km and ~ 10 km, respectively (Fig. 2). The northern sub-basin is presently used as an irrigation reservoir and an artificial dam separates this from the southern natural part of the basin. During the summer months the deepest part of the southern sub-basin fills with water to a depth of < 1 m.

The bedrock of the basin is composed of Cretaceous to Quaternary metamorphic, igneous, and sedimentary rocks (Nieto-Samaniego et al., 2012). Paleogene rhyolite and ignimbrite are the dominant lithology and are exposed in the ~ 2500–3000 m high mountains to the immediate east and west of the basin. A large outcrop of Pliocene–Pleistocene basalt is present ~ 20 km southeast of the basin, constituting the second most important lithology. Minor exposures of Paleogene andesite are present in the surroundings. The Quaternary deposits consist of lacustrine sediments and alluvium.

Modern climate

A meteorological station at the western margin of the Santiaguillo Basin (at Guatimape, Fig. 2) recorded an average annual precipitation of ~ 430 mm between AD 1951–2010 (Source: Servicio Meteorologico Nacional, Mexico). Summer and autumn precipitations (June–October) associated with the NAM and tropical cyclones contributed almost 90% (~ 385 mm) of the annual rainfall; the winter precipitation (November–March) contributes < 10% of the annual total. Average annual temperature is ~ 18°C; it can reach ~ 34°C during the months of May–June and is sub-zero during December–February.

Sampling and analysis

Sediments were collected up to the depth of 300 cm in a pit dug in the modern shore of the southern sub-basin (Fig. 2). Chronology of the sediment column is based on 6 AMS ^{14}C ages on organic matter present in the bulk sediments collected at depths of 49, 73, 111, 167, 205, and 279 cm (Fig. 3, Table 1). Samples at 2 cm intervals ($n = 150$) were oven dried at 40°C, homogenized and ground with an agate pestle. Concentrations of total carbon and inorganic carbon (IC) were determined at ~ 4–6 cm intervals ($n = 61$) in a Thermo Scientific HiperTOC solid analyzer. Organic carbon (OC) content was calculated by subtracting IC from total carbon and we expressed IC as carbonate (CO_3). Total nitrogen (TN) was measured at ~ 10 cm intervals ($n = 31$) in a Perkin Elmer Series II CHNS/O elemental analyzer.

The concentrations of Ti, Fe, K, Ca, Sr, and Zr were measured in all samples using a Thermo Scientific Niton XL3t X-ray fluorescence (XRF) analyzer. The data were corrected after measuring the same elements in 61 samples using the traditional Siemens SRS 3000 XRF (e.g. Roy et al., 2012). Additionally, concentrations of Si, Al, Na, K, Ca and P were measured at ~ 4–6 cm intervals ($n = 61$) using traditional XRF. Low field magnetic susceptibility of all sediment samples was obtained using a Bartington MS2E high resolution surface scanning sensor at 2 kHz. A total of 8 different rock samples were collected from the two dominant lithologies (rhyolite and basalt) present in the watershed (see Fig. 2 for locations) and analyzed for major element concentrations using traditional XRF.

Results

Sediment

Sediment consists of silty-sand, silt, silty-clay and clay (Fig. 3). Intercalations of gray clay and yellow calcareous silt are evident at a depth of 300–278 cm. This is followed by massive yellow silt

https://doi.org/10.1016/j.yqres.2015.10.002 Published online by Cambridge University Press

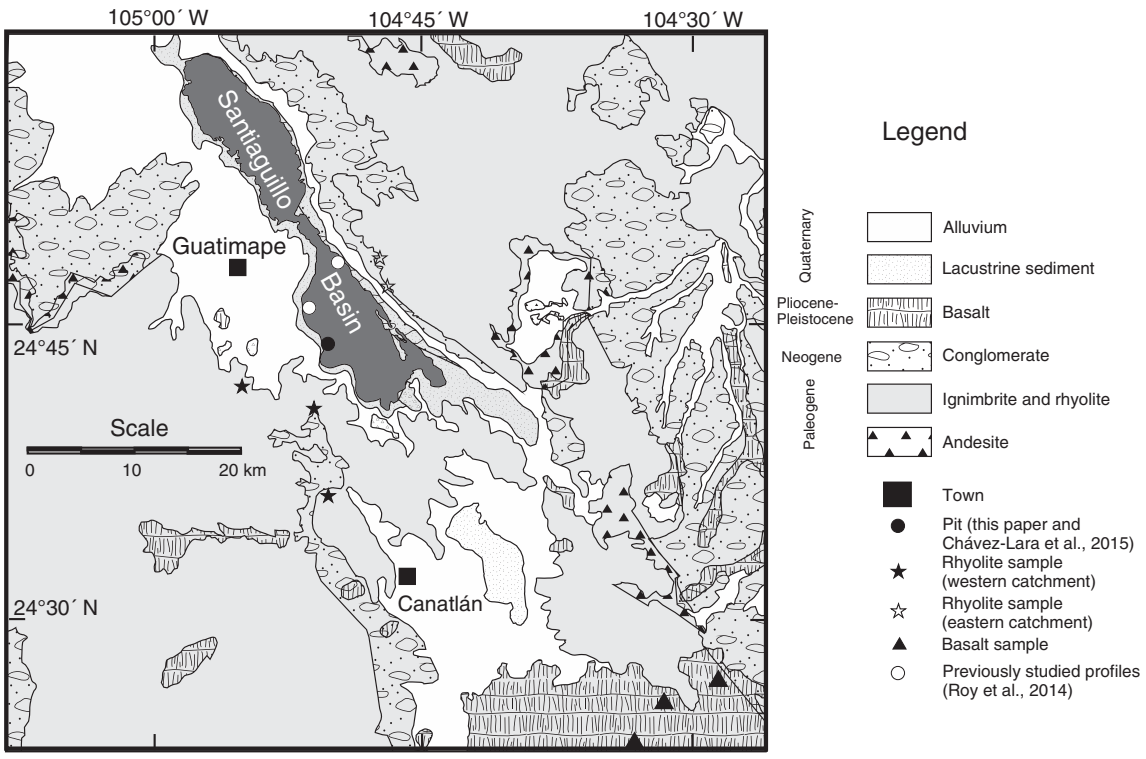

Figure 2. The geology of Santiaguillo Basin and sampling locations. A meteorological station at Guatimape provided the precipitation and temperature data between AD 1951–2010.

and silty-sand with occasional carbonate nodules to a depth of 75 cm. Intercalations of dark gray silty-clay and calcareous yellow silt occur above this zone to a depth of 50 cm, with vertical desiccation fissures (~ 65 cm long) at the depth of 75 cm. Massive dark gray silty-sand with abundant root remnants occur in the upper 50 cm.

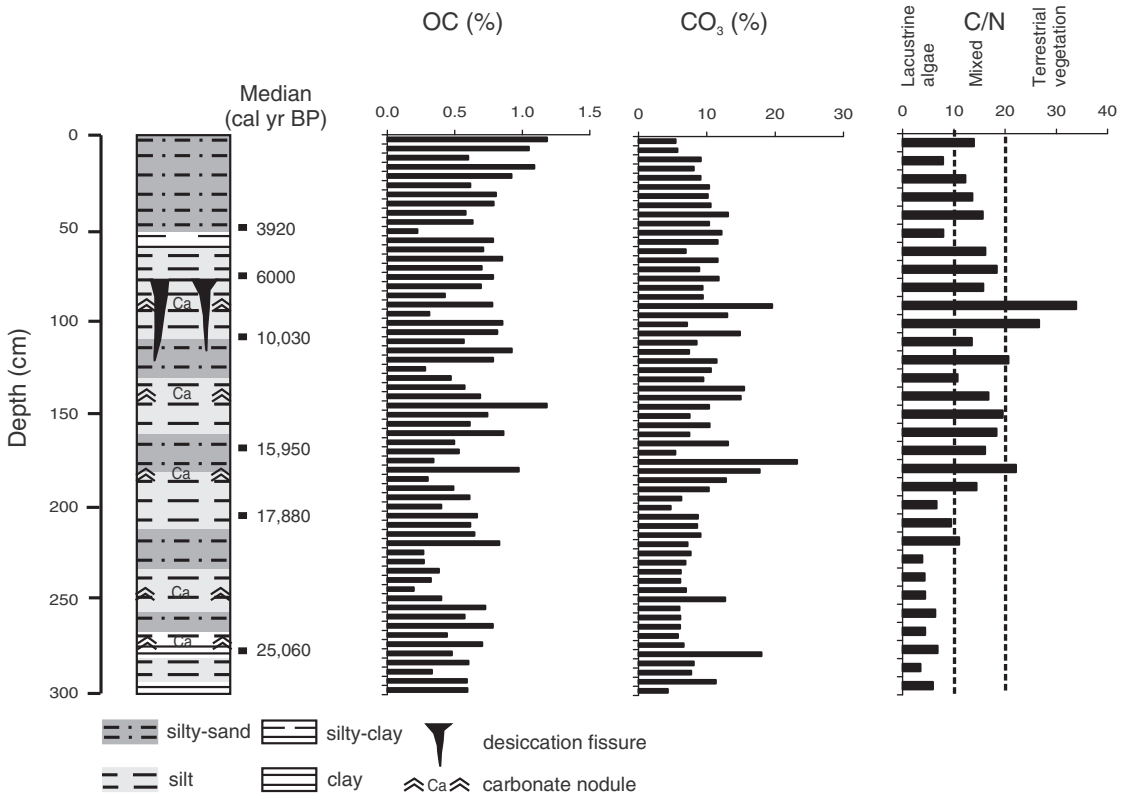

Figure 3. Stratigraphy of the sediment profile and median values of calibrated AMS ^{14}C ages at different depths. Distributions of organic carbon (OC), carbonate (CO_3) and organic carbon to total nitrogen relation (C/N) are presented along the depth.

https://doi.org/10.1016/j.yqres.2015.10.002 Published online by Cambridge University Press

Table 1
Radiocarbon ages of bulk sediment samples and calibration results for the Bayesian age–depth model constructed for a sediment succession from the Santiaguillo Basin.

Lab. code	Depth (cm)	$\delta^{13}C$ (‰)	Conventional age (±1σ, yr BP)	Modeled calibrated age[a] (2σ, cal yr BP)	Median (cal yr BP)	Agreement Index[b] (%)
Beta-299072	49	−18.0	3610 ± 30	3830–4060	3920	99.7
Beta-299073	73	−19.3	5250 ± 30	5920–6180	6000	96.2
Beta-321663	111	−20.2	8900 ± 40	9890–10190	10,030	100.2
Beta-299074	167	−20.8	13,360 ± 60	15,750–16,160	15,950	70.8
Beta-299075	205	−20.7	14,610 ± 60	17,690–18,040	17,880	87.4
Beta-299076	279	−20.9	20,790 ± 100	24,590–25,380	25,060	98.1

[a] Calibration using OxCal 4.2 (Bronk Ramsey, 2009) and IntCal_13 radiocarbon calibration curve (Reimer et al., 2013).
[b] Agreement Index for the model = 79.6%.

OC and CO_3

OC content ranges from 0.2 to 1.2% and the amount of CO_3 ranges between 4 and 23% (Fig. 3). Higher values of CO_3 at depths of 281 cm (18%, n = 1), 181–175 cm (18–23%, n = 2), 141–135 cm (15–16%, n = 2) and 91 cm (20%, n = 1) are characterized by occasional carbonate nodules. The distributions of OC and CO_3 do not show any significant correlation ($r = 0.1$, $p < 0.05$).

TN and C/N ratio

TN varies between 0.02 and 0.10% and sediments have C/N (OC/TN) of 3–34 (Fig. 3). Lower and less variable C/N (≤10) values characterize the sediment at depths between 200 and 300 cm. In general, C/N is variable (≥10) in sediments from a depth of 200 cm to the surface. Lower values are associated with sediments deposited at depths of 51 cm and 11 cm (C/N = 8) and the highest value is observed in sediments at a depth of 91 cm (C/N = 34).

Chronology

An age–depth model (Fig. 4) was generated using the online OxCal version 4.2 (Bronk Ramsey, 2009). The Bayesian age model is constructed using 6 different stratigraphically consistent ^{14}C ages, IntCal13 calibration curve (Reimer et al., 2013) and P sequence with k = 1 (Bronk Ramsey, 2008). Both the age model and calibrated ages were evaluated by the Agreement Index (A). This index is a measure of the correspondence between the data and model. More than 60% threshold for both indicates agreement between the age–depth model and observations, and suggests that there are no outliers within the radiocarbon ages. The calibrated ages and corresponding median values are presented in Table 1.

The age model incorporates uncertainties (1σ) of 44–195 years between the tie points and up to 480 years while extrapolating to bottom of the core at a depth of 300 cm. The model assigns a median age of ~27 ka to the base of sediment succession and estimates sedimentation of 9.4–19.8 cm/ka. The rate of sedimentation was highest (19.8 cm/ka) during ~17.8–15.9 ka and lowest (9.4 cm/ka) during ~15.9–6 ka. Sediments between depths of 49 and 300 cm were deposited between ~27 and 4 ka and sediments at depths from 49 cm to the surface represent the depositional history of last ~4 cal ka. Desiccation fissures at a depth of 75 cm suggest that the pit site was dry at ~6.5 ka. The comparable rates of sedimentation in the interval involving the desiccation (9.4 cm/ka) and two other intervals without any desiccation fissure, during ~25–17.8 ka (10.3 cm/ka) and ~10–6 ka (9.4 cm/ka) possibly suggest the absence of any hiatus or significant erosion at ~6.5 ka. However, the presence of hiatus and erosion of sediments in arid settings are common and the sediment profile representing the past 27 ka possibly contain many such events that were not detectable in the age model. The median calibrated age (with 1σ uncertainty) was assigned to sediments at 2 cm depth intervals using the interpolation option of OxCal.

Multi-element geochemistry

Basalt present to the southeast of the basin has Ti and Al concentrations of 1.8–2.3% and 3.9–4.3%, respectively. Rhyolite present in the east and west of the basin has Si concentrations of 34–37%. There are geochemical dissimilarities among the rhyolites. Rhyolite in the western catchment, for example, has more Ti (0.2–0.3%) and Al (3.4–3.7%) and less Si (34–35%) compared to the rhyolite in the eastern catchment. Rhyolite from the eastern catchment has 0.1% of Ti, 2.6–2.9% of Al and 37% of Si. The lacustrine sediments have Si concentrations of 21–31%, Al concentrations of 2.5–4.1% and Ti concentrations of 0.10–0.25%.

Degree of chemical alteration of the rocks and sediments is estimated by calculating the chemical index of alteration (CIA; Nesbitt and Young, 1984, 1989). CIA values of sediments and rocks are 48–86 and 43–55, respectively. Sediments in general have CIA ≥ 60 because most of them have undergone some degree of chemical weathering (Fig. 5A). Lower values (CIA < 60) at depths of 218, 251 and 91 cm

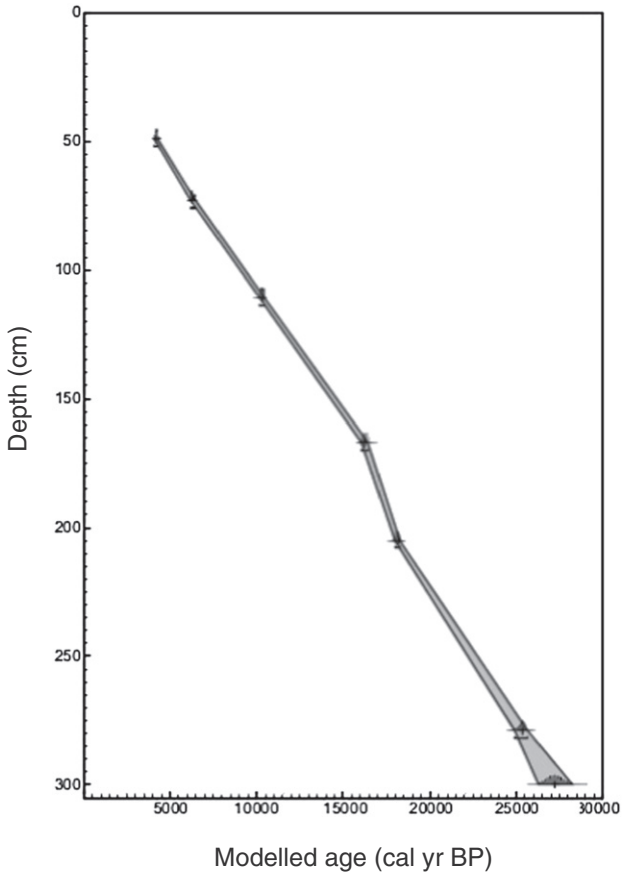

Figure 4. Age–depth model generated for the sediment profile using OxCal version 4.2.

https://doi.org/10.1016/j.yqres.2015.10.002 Published online by Cambridge University Press

represent events of deposition of unaltered to low altered sediments from the watershed into the basin. Irrespective of different degrees of chemical alteration, the linear trend of sediments in the A–CN–K ternary diagram indicates a uniform provenance over the past 27 ka. Presence of rhyolite samples collected from the western catchment along and close to the linear trend suggests that the lacustrine sediments were mainly sourced from erosion of the western rhyolite. Similarities in geochemical characteristics between the lacustrine sediments and western watershed rhyolite are also evident in the TiO_2/Al_2O_3 vs. SiO_2/Al_2O_3 binary plot (Fig. 5B). Both the lacustrine sediments and rhyolite from western watershed have comparable SiO_2/Al_2O_3 and TiO_2/Al_2O_3 values.

Concentrations of Ti, Fe, K, Ca, Sr, and Zr and relations of SiO_2/Al_2O_3 and Zr/Ti along the depth are presented in Figure 6. In general, both K (2.3–3.2%) and Zr (110–209 ppm) are similar to Ti ($r = 0.8$, $p < 0.05$) and represent the abundance of clastic sediment. Distribution of Ca (1.8–15.2%) is comparable ($r = 0.9$, $p < 0.05$) to CO_3 (Fig. 6) and it represents the abundance of carbonate minerals. Both Fe and Sr have distinct temporal distributions ($r = 0.4$, $p < 0.05$). Distributions of Fe and Ti are similar in some parts of the sediment profile and opposite in other parts ($r = 0.1$, $p < 0.05$). Occurrence of Fe, both in clastic grains and carbonate, could be due to the mobilization of Fe from the silicates and oxides in an anoxic environment and precipitation along with carbonate during the intervals of higher salinity (Cohen, 2003). Similarly, Sr is associated with both clastic grains (300–200 cm) and carbonate (200–0 cm). The strong positive correlation between Ti and Zr ($r = 0.8$, $p < 0.05$) suggests that both are present in the Ti-bearing and Zr-bearing clastic sediment sourced from erosion of the western rhyolite. The rhyolitic source of Ti and Zr is also suggested by similar temporal variations of Ti, Zr and SiO_2/Al_2O_3 ($r = 0.5$, $p < 0.05$). However, Zr/Ti values are variable along the depth ($670–1090 \times 10^{-4}$) and suggest that the basin received more Zr-bearing clastic grains compared to Ti-bearing clastic grains during certain intervals (e.g. sediments at 200–85 cm depth).

Magnetic susceptibility

Magnetic susceptibility values range between 6 and 17×10^{-5} SI (Fig. 6). Characterized with high amplitude variations, the sediments from a depth of 300–223 cm have higher values ($10–17 \times 10^{-5}$ SI). Intermediate values ($11–12 \times 10^{-5}$ SI) are associated with the sediments at a depth of 155–147 cm. The upper 85 cm of the sediment column have lower values ($6–10 \times 10^{-5}$ SI). In general, the distribution of magnetic susceptibility is similar to Ti ($r = 0.6$, $p < 0.05$) and inverse of Ca ($r = -0.5$, $p < 0.05$). More Ti-bearing clastic sediments were deposited during the intervals of higher magnetic susceptibility, whereas more carbonates were precipitated during the intervals with lower magnetic susceptibility.

Discussion

Proxy

Concentrations of Ti and Ca, ratios of Zr/Ti and C/N, and calculated CIA values are used as proxies to document the paleohydrological variations (Fig. 7). CIA estimates chemical alteration of sediments and is used here as an indicator of the degree of sediment–water interaction in the watershed. In the absence of any carbonate-bearing rock in the watershed, the carbonate enriched sediments are related to intervals of more saline water and thus more evaporative/drier conditions in the basin. Both Ca and CO_3 have similar distributions and we consider that the sediments with more Ca represent intervals of more saline water and evaporative conditions. Ti reflects the contribution of detrital materials into the basin. The uniform provenance over the last 27 ka suggests that sediments with more Ti represent intervals of greater clastic deposition. Negative coefficient of correlation between Ti and Ca ($r = -0.9$, $p < 0.05$) suggests that more Ti-bearing clastic sediment were deposited during intervals of less saline water and thus less evaporative/wetter conditions. In general, sediments with more Ti are characterized by CIA of ≥60. Moderate to highly altered sediments were transported from the watershed into the basin via runoff as recorded by higher Ti values. Consequently, we use Ti as a proxy to estimate runoff into the basin. Sediments with more Ti were deposited during the intervals of more runoff during wetter climates and vice versa.

The moderate positive relationship between Zr/Ti and Ca ($r = 0.4$, $p < 0.05$) suggests that more Zr-bearing clastic sediments were deposited during the intervals of more saline water and more evaporative/drier

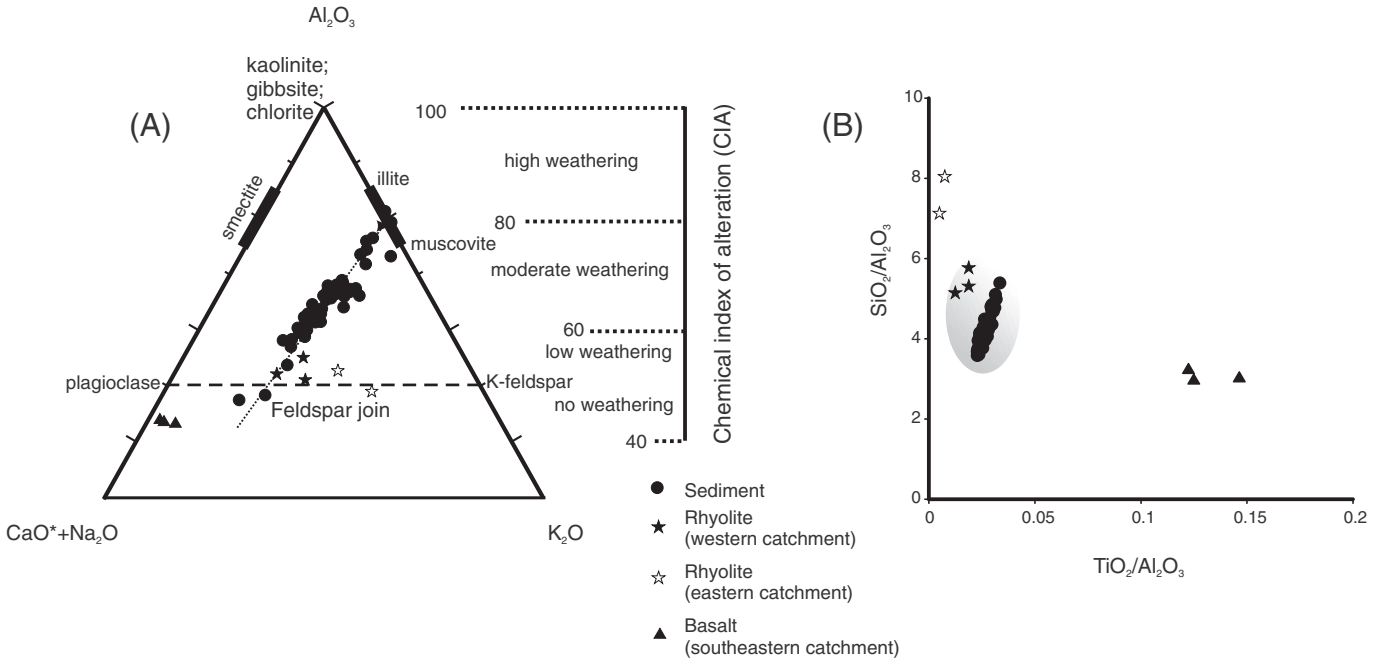

Figure 5. (A) Ternary diagram showing molar proportions of Al_2O_3, ($CaO^* + Na_2O$) and K_2O and the scale of chemical index of alteration (CIA) of sediments and rocks. (B) Binary plot of TiO_2/Al_2O_3 vs. SiO_2/Al_2O_3 in sediments and rocks.

https://doi.org/10.1016/j.yqres.2015.10.002 Published online by Cambridge University Press

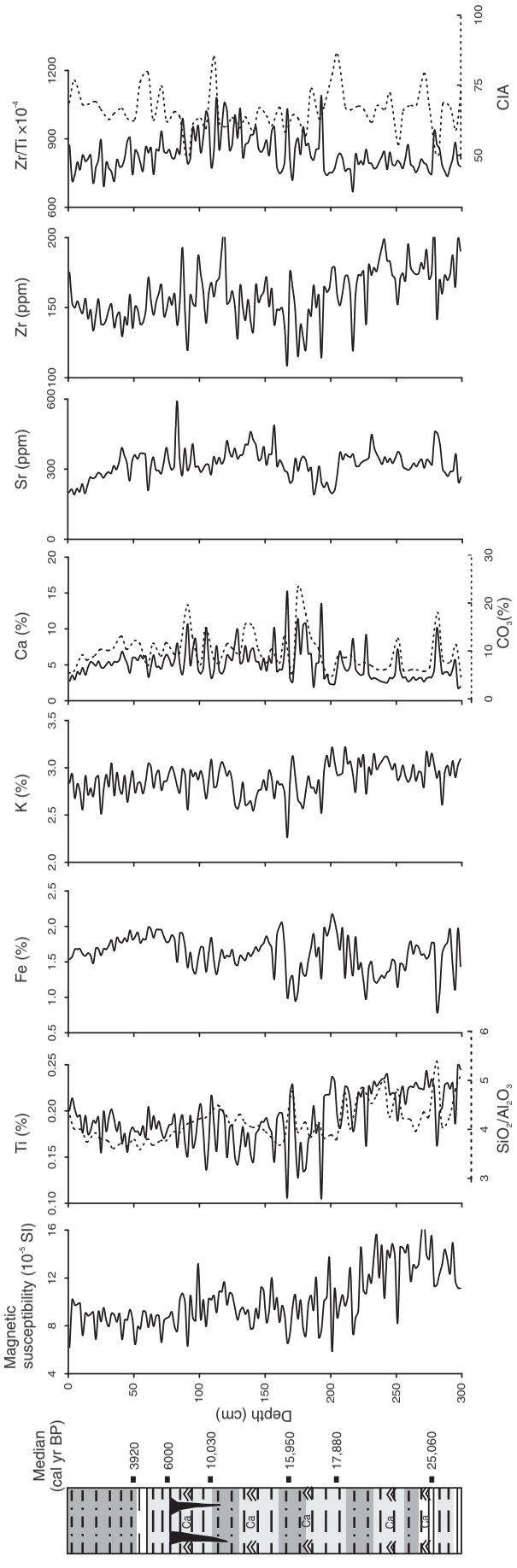

Figure 6. Distributions of magnetic susceptibility, concentrations of Ti, Fe, K, Ca, Sr, and Zr, CIA and ratios of SiO_2/Al_2O_3 and Zr/Ti along the depth. The distributions of Ti and Zr are similar to the variations of SiO_2/Al_2O_3. Both Ca and CO_3 have similar tendencies with depth.

https://doi.org/10.1016/j.yqres.2015.10.002 Published online by Cambridge University Press

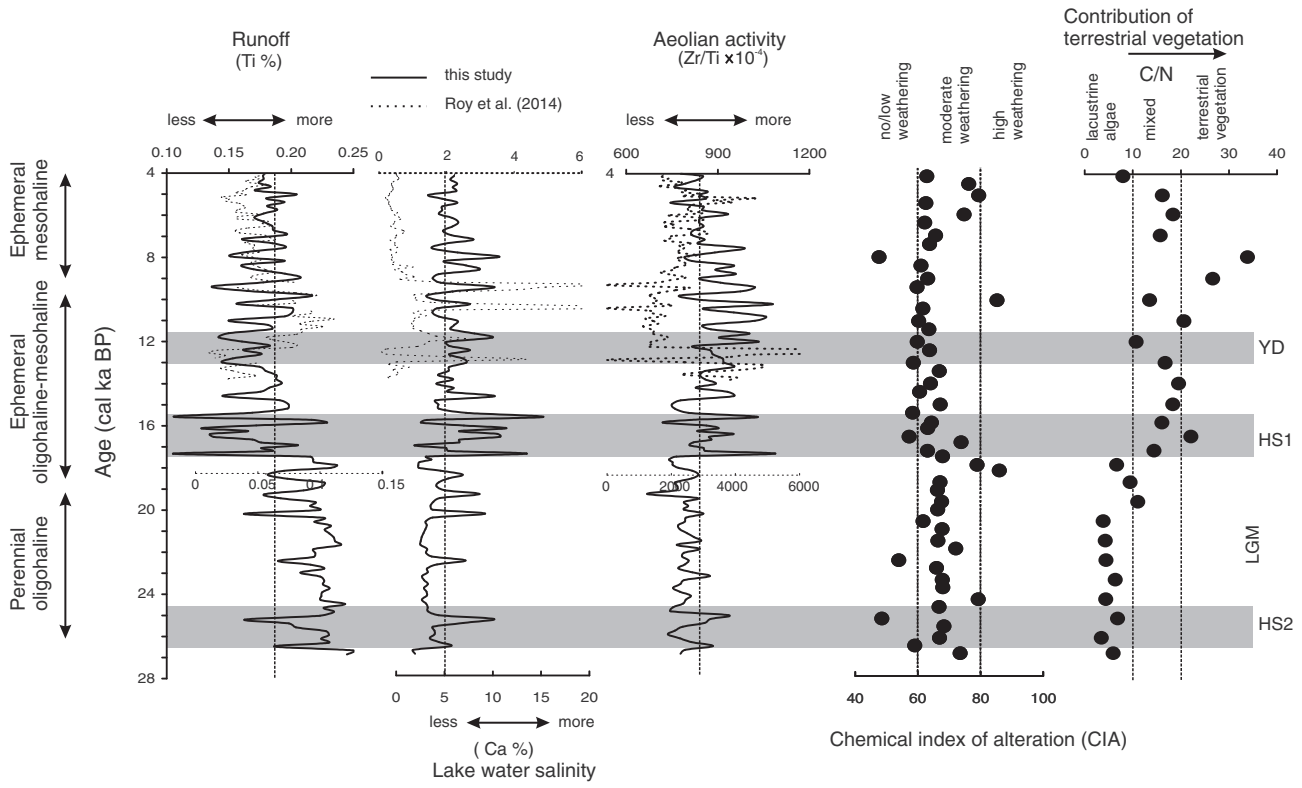

Figure 7. Proxy records indicating variations in runoff (Ti), lake water salinity (Ca) and aeolian activity (Zr/Ti) during ~27–4 ka. Sediment–water interaction in the watershed is estimated from CIA values and the source of sediment organic matter is inferred from C/N relation. The dotted lines show average values of Ti, Ca, and Zr/Ti. Heinrich 2 (HS2) and 1 (HS1), and Younger Dryas (YD) stadials are represented by dark gray bands.

conditions. Sediments with higher values of Zr/Ti are characterized by CIA of ≤60. Zr-bearing clastic sediments along with minimally altered sediments were transported from the dry watershed by aeolian processes. Therefore, the ratio of Zr/Ti is used to infer aeolian activity. Contributions of terrestrial vegetation and lacustrine algae to the organic matter deposited in the basin are determined from C/N relation. Lacustrine algae are characterized by C/N < 10, whereas terrestrial plants are characterized by C/N > 20. Mixed contribution from lacustrine algae and terrestrial vegetation is reflected by C/N values between 10 and 20 (Talbot and Johannessen, 1992; Meyers and Ishiwatari, 1995).

The proxy data and interpretations are shown in Figure 7, but we do not provide paleohydrological reconstructions of the past 4 ka due to lack of chronological control in the upper part of the sediment column. The proxy records are compared with paleoecological data obtained from ostracod species assemblages from the same profile (Chávez-Lara et al., 2015). Concentrations of Ti, Ca and Zr/Ti ratio from another shallow core reported in Roy et al. (2014) are also shown along with our data (Fig. 7). Except for the Zr/Ti ratio, the variations of Ti and Ca are comparable between ~ 14 and 4 ka. Sediments with higher Ti in the shallow core (~ 12.3–9.3 ka; Roy et al., 2014) and pit (~11.5–9 ka; this paper) were deposited during contemporary intervals. Similarly, higher values of Ca in the shallow core sediments are present at ~13, 12, 10.5 and 9.5 ka (Roy et al., 2014) and above average Ca concentrations are observed in the pit sediments at ~13, 12, 10 and 9.5 ka. The slight offsets could be due to chronology of the interpolated parts of age models. Variation in Zr/Ti ratio is different in the previously published shallow core and the present study. Both records indicate higher values between ~ 14 and 12.3 ka. However, the above average Zr/Ti between ~ 12.3–7.5 ka is only registered in the pit sediments and not in the shallow core. The difference could be due to aeolian transported Zr-bearing clastic grains not reaching uniformly to all sites within the basin. The pit site possibly recorded more intervals of aeolian activity due to its location in the basin margin, whereas the shallow core location received aeolian transported minerals only during some of the arid intervals.

Paleohydrological variation at Santiaguillo

Santiaguillo Basin received generally above average runoff between ~27 and 18 ka (Fig. 7). Aeolian activity around the basin was generally below average. Deposition of mostly moderate to highly altered sediments reflects more sediment–water interaction in the watershed during the late last glacial. C/N values of ≤10 indicate that the organic matter was dominantly sourced from lacustrine algae. Lower C/N along with above average Ti suggests that algal productivity increased during this interval of more runoff into the basin. Ostracod assemblage indicates presence of a diluted and perennial oligohaline water column at the modern dry pit site during the late last glacial and LGM (Chávez-Lara et al., 2015). However, the sediments deposited at ~ 26.5 ka and ~25 ka indicate brief events of average and below average runoff, enhanced aeolian transportation of Zr-bearing minerals, above average evaporative conditions and deposition of minimally altered sediments. Both the events of reduced runoff and above average aeolian activity occurred within the Heinrich Stadial 2 (26.5–24.3 ka; Sanchez Goñi and Harrison, 2010). Other similar short lived intervals of more evaporative/drier conditions at ~22.5, 20, 19, and 18.5 ka characterize the late last glacial (Fig. 7).

Except for 3 brief events between ~11.5 and 9 ka, runoff into the basin was average and below average between ~18 and 4 ka. C/N values of >10 indicate that the organic matter in the sediment was dominantly sourced from terrestrial vegetation during the deglaciation and Holocene. Terrestrial vegetation encroached into the modern littoral zone of the basin in this interval of reduced runoff. The ostracods suggest increased lake water salinity and presence of an ephemeral oligohaline to mesohaline water column at the pit site (Chávez-Lara et al., 2015). Changing hydrological conditions during this interval are reflected by

https://doi.org/10.1016/j.yqres.2015.10.002 Published online by Cambridge University Press

high amplitude variations in proxy records. Sediment–water interaction and its effect on weathering in the watershed were low–moderate between ~17 and 10.5 ka, and increased to moderate–high during ~ 10.5 to 9 ka and ~7 to 4 ka.

Two notable intervals of below average runoff occurred during ~17.5–16 ka and ~13–11.5 ka, and are coincident with Heinrich Stadial 1 (18–15.6 ka; Sanchez Goñi and Harrison, 2010) and the Younger Dryas Stadial (12.8–11.6 ka; Pettet, 2009). Both the intervals are represented by above average carbonate precipitation and aeolian activity. In summary, our data indicate a transition from wet late last glacial and LGM to a drier deglaciation and Holocene occurred at ~18 ka. Superimposed on this first order change in hydrologic conditions are the short-lived excursions in aridity and wetness.

Runoff into Santiaguillo Basin and seasonality of precipitation

To evaluate influences of different precipitation sources on the hydrological variations that occurred since the late last glacial, the new runoff record from the Santiaguillo Basin is compared with high-resolution records of monsoonal rainfall reconstructed from oxygen isotope composition of a speleothem from the Juxtlahuaca Cave (Lachniet et al., 2013) and winter precipitation reconstructed from sand contents in sediments from the Lake Elsinore (Kirby et al., 2013) (Fig. 8). Both these sites represent end members of the hydroclimatic regime. The speleothem reconstructs variations in amounts of monsoonal rainfall over the last 22 ka in the southwestern Mexico and the sand contents reconstruct variation in amounts of winter precipitation between 19 and 9 ka in the coastal southwestern US.

Runoff into Santiaguillo Basin and the $\delta^{18}O$ values from the speleothem have similar oscillations on millennial time scales. However, Ti concentrations of Santiaguillo Basin sediments and sand contents of Lake Elsinore are inversely related. Enhanced monsoonal precipitation in the southwestern Mexico between 22–18 ka occurred within the interval of generally above average runoff into Santiaguillo between ~27 and 18 ka. Similarly, the regime of weaker monsoonal precipitation during 17.5 to 11 ka was contemporary to the interval of generally below average runoff into Santiaguillo at ~ 18–11.5 ka. Over a large part of this interval, ~ 19–12.9 ka, the coastal southwestern US recorded enhanced winter precipitation. We suggest that runoff into the Santiaguillo Basin was mainly controlled by the monsoonal precipitation and winter rainfall was not a significant contributor. The southern part of western subtropical North America received more monsoonal precipitation during the late last glacial and LGM (~ 27–18 ka). The amount of monsoonal rainfall decreased over the deglaciation into the Pleistocene–Holocene transition (~ 18–11.5 ka).

Regional hydrological variation

Paleoclimate records from 9 different sites from the northern and northwestern Mexico (Blanchet et al., 2007; Roy et al., 2010, 2012), US–Mexico borderland (Holmgren et al., 2007) and coastal (Kirby et al., 2006, 2013) and continental interiors of southwestern US (Anderson et al., 2002; Asmerom et al., 2007, 2010; Wagner et al., 2010) are compared to evaluate the millennial-scale changes in hydroclimate during intervals of ~ 27–18 and 18–10 ka in Figure 9.

Between ~ 27 and 18 ka, more monsoonal precipitation in the central-northern Mexico provided above average runoff into Santiaguillo Basin. The enhanced aeolian activity in Baja California Peninsula and reduced runoff into the lacustrine basins of Babicora and San Felipe suggest that northern and northwestern Mexico remained drier. Lack of macrofossils of summer flowering annuals and C_4 grasses in packrat middens from the Peloncillo and Hueco Mountains (i.e., US–

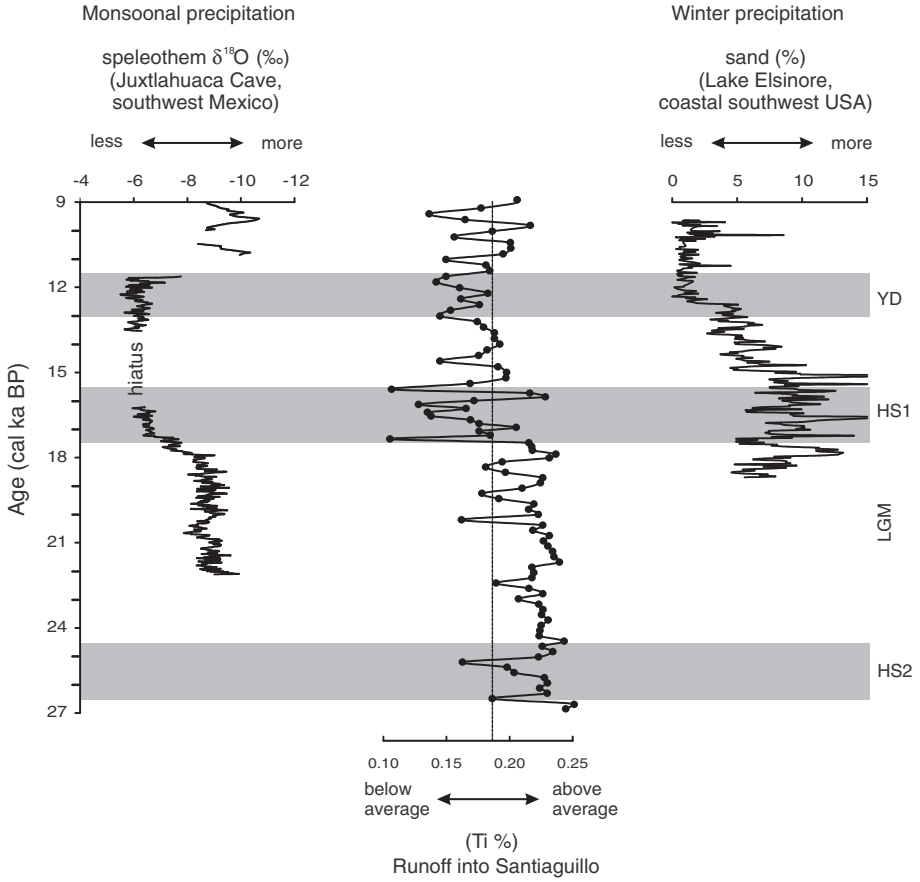

Figure 8. Comparison of runoff into Santiaguillo Basin with the proxy records of monsoonal precipitation estimated in a speleothem from Juxtlahuaca Cave (Lachniet et al., 2013) and winter precipitation estimated from sand contents in sediments of Lake Elsinore (Kirby et al., 2013). The dotted line indicates average Ti value of Santiaguillo Basin sediments.

https://doi.org/10.1016/j.yqres.2015.10.002 Published online by Cambridge University Press

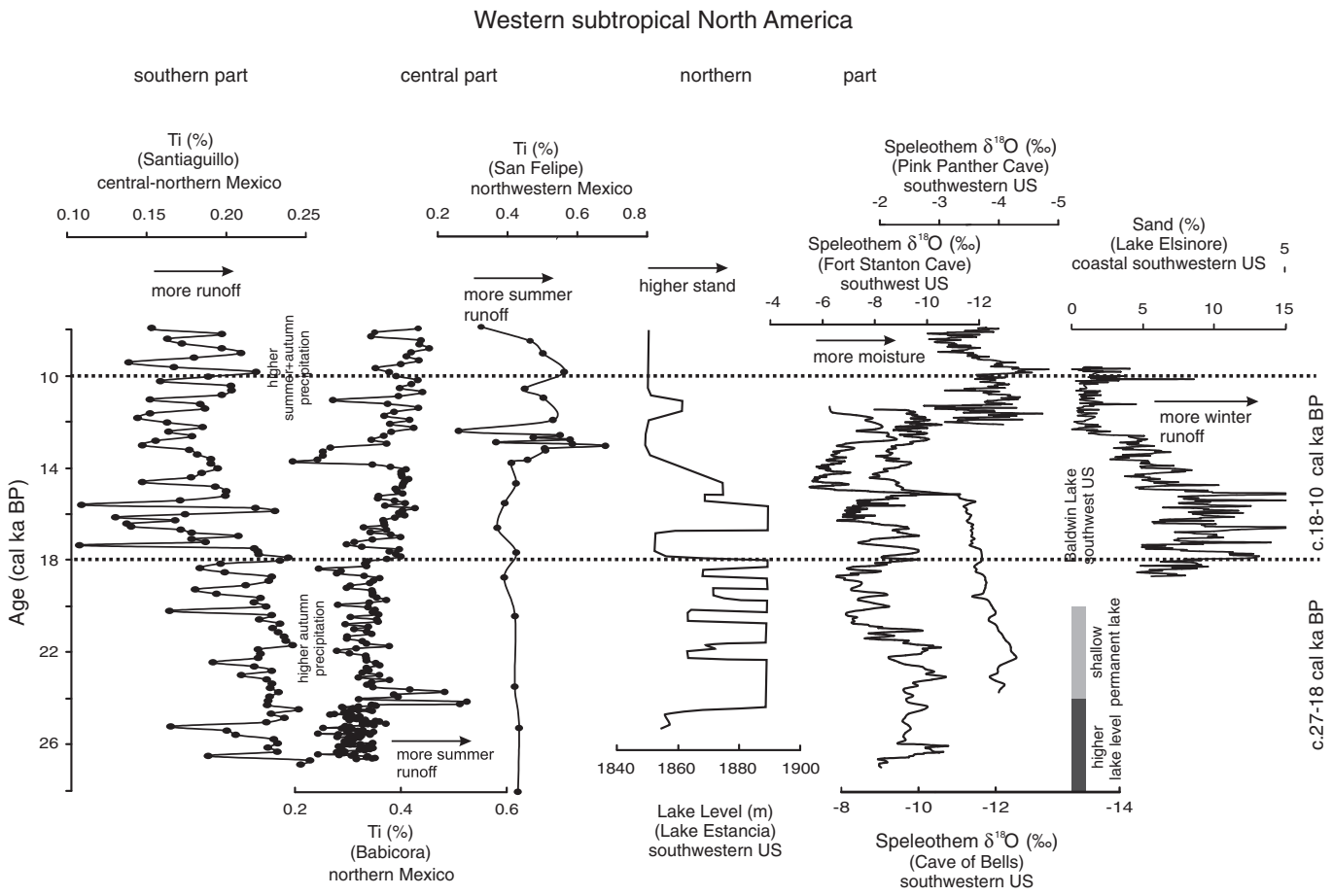

Figure 9. Regional hydrological variation estimated by comparison of proxy-records of runoff into the lacustrine basins of central-northern, northern and northwestern Mexico (Roy et al., 2010, 2012, this study), speleothem records of moisture variation in southwestern US (Asmerom et al., 2007, 2010; Wagner et al., 2010) and lake-level variations in coastal (Kirby et al., 2005, 2006, 2013) and continental interiors of southwestern US (Anderson et al., 2002) between ~27 and 10 ka. The grouping of registers in terms of southern, central and northern parts is based on location of the comparison sites.

Mexico borderland) suggests that little monsoonal precipitation fell at higher latitudes. However, the enhanced winter precipitation led to the development of permanent lakes in the coastal southwestern US (i.e. Baldwin Lake; Kirby et al., 2006). In a regime of monsoonal precipitation restricted to the central-northern Mexico, we relate the varying moisture contents in the continental interiors of southwestern US to different amounts of winter precipitation. More winter precipitation led to higher lake stands at Lake Estancia (Anderson et al., 2002) and more humidity in the Cave of Bells and Fort Stanton Cave (Asmerom et al., 2010; Wagner et al., 2010).

Between ~18 and 10 ka, the generally drier conditions of Santiaguillo Basin indicate reduction in monsoonal precipitation in the central-northern Mexico. However, more summer precipitation in the northern Mexico provided increased runoff into Babicora after ~18 ka. Similarly, more summer precipitation was occurring in the Peloncillo and Hueco Mountains. This wetter climate over a broad region decreased the aeolian transported terrigenous material from the southern Baja California peninsula into the Pacific Ocean. Higher lake stand in Lake Estancia (~17–14 ka; Anderson et al., 2002) and more moisture in Fort Stanton Cave (18–15 ka; Asmerom et al., 2010) were contemporary to an interval of more winter precipitation in the coastal southwestern US as well as higher summer precipitation in northern Mexico. During the interval of lowest winter precipitation in coastal southwestern US at ~12.9–10 ka (Kirby et al., 2013), more moisture in Cave of Bells (13–11.5 ka; Wagner et al., 2010) and Pink Panther Cave (12.3–10 ka; Asmerom et al., 2007), higher stand of Lake Estancia (~ 12–11 ka; Anderson et al., 2002) and more runoff into San Felipe (~13–10 ka; Roy et al., 2010) and Santiaguillo (~ 11.5–9 ka) can only be explained by higher amounts of monsoonal/summer precipitation. We conclude that the monsoonal/summer precipitation gradually expanded to higher latitudes over the deglaciation and reached one of its greatest spatial extents during the Pleistocene–Holocene transition and early Holocene.

Forcing

Based on the Holocene records, Metcalfe et al. (2015) reported that both summer as well as autumn insolation influenced monsoonal precipitation of the NAM region. The modern summer precipitation is associated with NAM and the moisture flow is sourced from GoC and GoM (Adams and Comrie, 1997; Mitchell et al., 2002). Both the instrumental and proxy records indicate positive correlations between NAM and SST of both GoC and GoM (Mitchell et al., 2002; Barron et al., 2012; Metcalfe et al., 2015). Similarly, the northerly-located ITCZ in boreal summer strengthens the NAM (Amador et al., 2006). Figure 10 compares different forcings with proxy precipitation record for the Santiaguillo Basin to help identify the possible moisture sources.

Except for Heinrich 1 and Younger Dryas stadials, the temporal variations in runoff show a first order negative correlation with mean position of ITCZ. Similarly, the influences of summer (June) insolation and North Hemisphere temperature on runoff were minimal. More runoff between ~27–18 ka was contemporary to a southerly positioned ITCZ, lower summer insolation and cooler temperature in the North Hemisphere. The amount of runoff decreased over the deglaciation as the

https://doi.org/10.1016/j.yqres.2015.10.002 Published online by Cambridge University Press

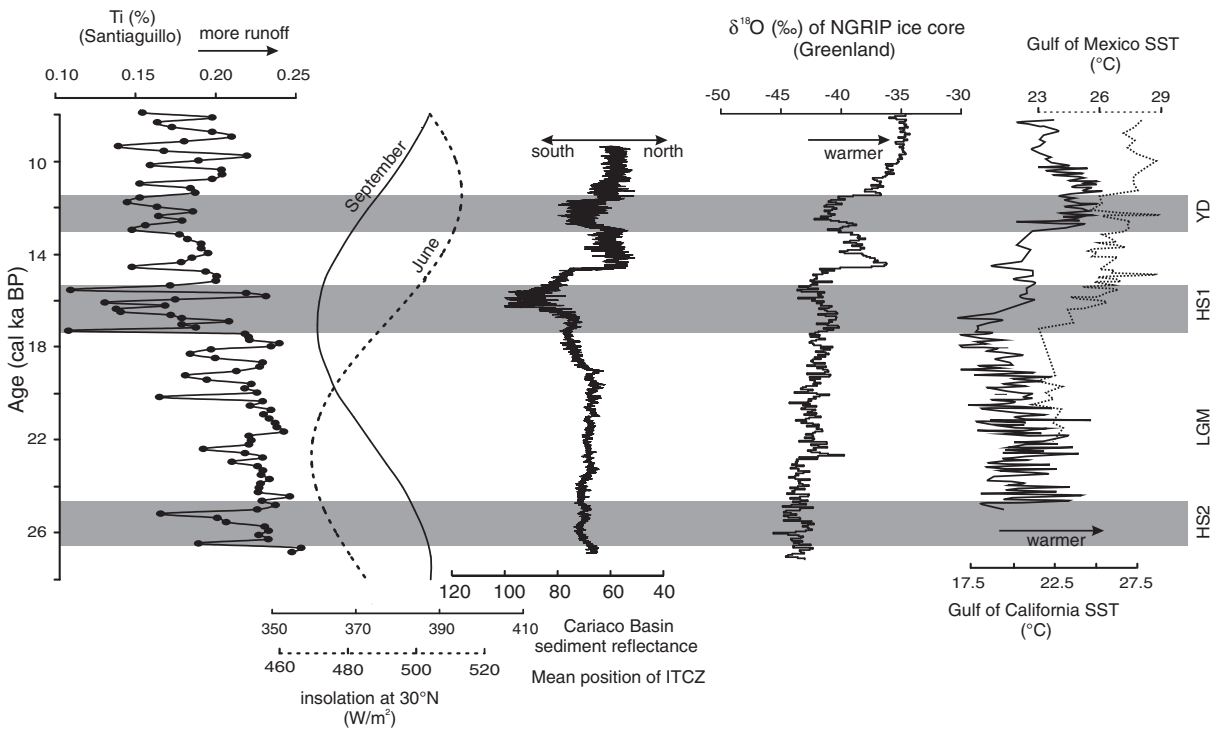

Figure 10. Evaluation of possible forcings on the variable monsoonal precipitation in the southern part of western subtropical North America by comparing the proxy record of runoff into the Santiaguillo Basin with June and September insolations at 30°N latitude (Berger and Loutre, 1991), reconstructed North Hemisphere temperature (NGRIP project members, 2004), mean position of ITCZ (Deplazes et al., 2013) and SST records from Gulf of California (McClymont et al., 2012) and Gulf of Mexico (Flower et al., 2004).

ITCZ shifted northward, summer insolation increased and North Hemisphere became warmer. A proxy SST record from the Guaymas Basin indicates that GoC did not have the precondition for NAM onset (i.e. ~26°C; Mitchell et al., 2002) during the late last glacial and deglaciation. The contrasts between runoff and another proxy SST record from the Orca Basin suggest that minimal amount of moisture reaching the Santiaguillo Basin was sourced from GoM. We propose that NAM was either absent or weaker during the late last glacial and deglaciation.

Tropical cyclones forming in the eastern North Pacific during the autumn provide an additional source of moisture for the region (Ritchie and Elsberry, 2007; Corbosiero et al., 2009; Ritchie et al., 2011). As the North Hemisphere summer progresses into the autumn, the interaction between mid-latitude upper-level troughs and northward moving tropical cyclones drop a large quantity of precipitation over Mexico and across the southwestern US (Jones et al., 2003). The runoff record for the Santiaguillo Basin shows a first order positive correlation with the autumn insolation (September). During the late last glacial and early Holocene, the Santiaguillo Basin received above average runoff and autumn insolation was higher. Runoff decreased (below average) in an interval of lower autumn insolation during the deglaciation. A compilation of the meteorological data during AD 1992–2005 by Ritchie et al. (2011) indicates that the highest numbers of tropical cyclones remnants were formed in September and the tropical cyclones had different rainfall swaths. Tropical cyclones grouped as a *south recurving track* (e.g. Hurricane Kenna, AD 2002) and *rain in Mexico only* (e.g. Hurricane Ileana, AD 1994) had rainfall swaths restricted to the central-northern Mexico. However, the tropical cyclones with a *north recurving track* (e.g. Hurricane Hilary, AD 1993) had expanded rainfall swaths and brought moisture into the northern-northwestern Mexico as well as continental interiors of southwestern US.

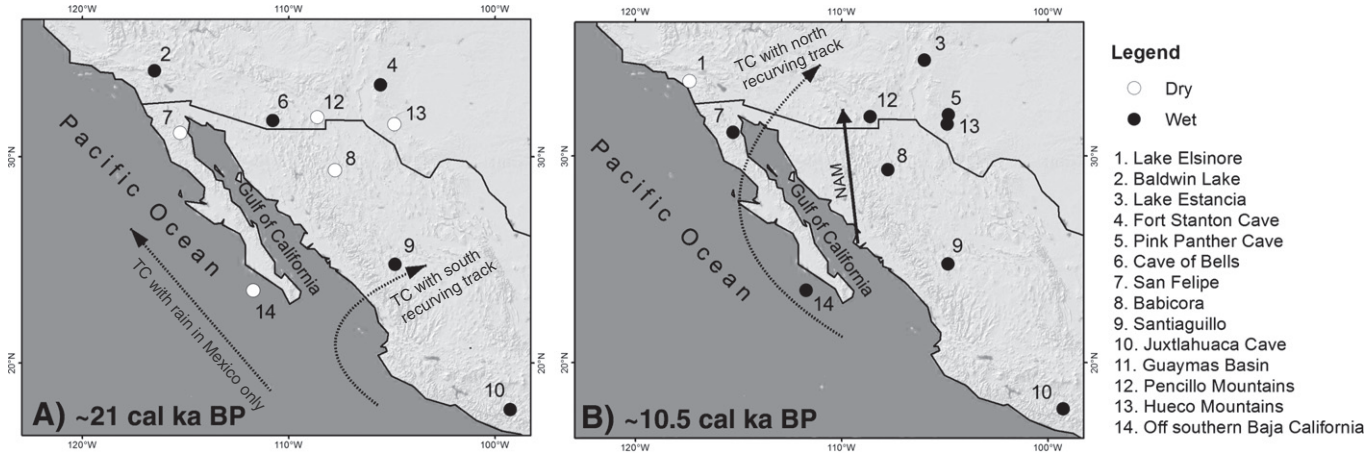

Figure 11. Map showing the regional hydroclimate at ~21 ka (A: LGM) and ~10.5 ka (B: early Holocene). Arrows indicate different modern tropical cyclone (TC) rainfall swath patterns transporting moisture from the eastern North Pacific (Ritchie et al., 2011) and North American Monsoon (NAM) transporting moisture from Gulf of California (Mitchell et al., 2002).

https://doi.org/10.1016/j.yqres.2015.10.002 Published online by Cambridge University Press

We chose to discuss the hydroclimate at ~21 ka (LGM) and ~10.5 ka (early Holocene) as both intervals had different moisture sources (Fig. 11). In the absence or occurrence of a weaker NAM, we relate the LGM wetter climate of the central-northern Mexico to frequent formation of tropical cyclones in the eastern North Pacific with restricted rainfall swaths. During the early Holocene, SST of GoC attended the precondition required for the NAM onset (Mitchell et al., 2002) and tropical cyclones increasingly penetration into the southwestern US (~ 11.5–9 ka; Antinao and McDonald, 2013). We assume that the occurrence of more rainfall in a broader region extending from the central-northern Mexico in the south up to the continental interiors of southwestern US in the north were caused by stronger NAM during the summer and tropical cyclones with expanded rainfall swaths during the autumn.

Conclusions

Geochemical characteristics of sediments in the Santiaguillo Basin provided information about runoff, evaporation and lake salinity, provenance of organic productivity and clastic sediments in the basin, and aeolian activity in the central-northern Mexico over the past 27 ka. Comparison of the proxy runoff record with pure end member sites suggests that the hydrological variations were controlled by the millennial-scale dynamics of summer and autumn precipitations related to the NAM and tropical cyclones. More specifically:

- A transition from wet late last glacial and LGM to a drier deglaciation and Holocene occurred at ~18 ka. Superimposed on this first order change in hydrologic conditions are the short-lived excursions in aridity and wetness. Runoff decreased during Heinrich 1 and 2, and Younger Dryas stadials. The deposition of authigenic carbonate and aeolian transported sediment increased during these arid intervals.
- Difference between the Santiaguillo runoff record and summer insolation (June), North Hemisphere temperature, mean position of ITCZ and SST records from the Gulf of California and Gulf of Mexico suggests that the NAM had minimal influence on the hydroclimate of late last glacial and deglaciation.
- Frequent formation of tropical cyclones in the eastern North Pacific with restricted rainfall swaths brought more autumn precipitation to the central-northern Mexico during the late last glacial. However, the absence or occurrence of a weaker NAM caused drier conditions in the northern–northwestern Mexico.
- During the early Holocene, an enhanced NAM and tropical cyclones with expanded rainfall swath patterns brought more summer and autumn moisture from the Gulf of California and eastern North Pacific to a broader region extending from the central-northern Mexico in the south up to the continental interiors of southwestern US in the north.

Acknowledgments

This research was supported by Papiit-UNAM IN100413 and Conacyt CB-237579. Technical assistance was provided by Patricia Girón García (IGL), Victor Lemus Neri (USAI), Fernando Nuñez and Marcela Charles Polo. Suggestions and comments of both the anonymous reviewers and Prof. Lewis Owen (editor) are thankfully acknowledged. Staffs of Heroico Cuerpo de Bomberos and Protección Civil of Durango provided assistance and security to the expedition members during field visits and sampling.

References

Adams, D.K., Comrie, A.C., 1997. The North American monsoon. Bulletin of the American Meteorological Society 78, 2197–2213.
Amador, J.A., Alfaro, E.J., Lizano, O.G., Magaña, V.O., 2006. Atmospheric forcing of the eastern tropical Pacific: a review. Progess in Oceanography 69, 101–142.
Anderson, R.S., Power, M.J., Smith, S.J., Springer, K., Scott, E., 2002. Paleoecology of a middle Wisconsin deposit from Southern California. Quaternary Research 58, 310–317.
Antinao, J.L., McDonald, E., 2013. An enhanced role for the Tropical Pacific on the humid Pleistocene–Holocene transition in southwestern North America. Quaternary Science Reviews 78, 319–341.
Asmerom, Y., Polyak, V., Burns, S., Rassmussen, J., 2007. Solar forcing of Holocene climate: new insights from a speleothem record, southwestern United States. Geology 35, 1–4.
Asmerom, Y., Polyak, V.J., Burns, S.J., 2010. Variable winter moisture in the southwestern United States linked to rapid glacial climate shifts. Nature Geoscience 3, 114–117.
Barron, J.A., Metcalfe, S.E., Addison, J.A., 2012. Response of the North American Monsoon to regional changes in ocean surface temperature. Paleoceanography 27, 1–17, PA3206.
Berger, A., Loutre, M.F., 1991. Insolation values for the climate of the last 10 million years. Quaternary Science Reviews 10, 297–317.
Blanchet, C.L., Thouveny, N., Vidal, L., Leduc, G., Tachikawa, K., Bard, E., Beaufort, L., 2007. Terrigenous input response to glacial/interglacial climatic variations over southern Baja California: a rock magnetic approach. Quaternary Science Reviews 26, 3118–3133.
Bromwich, D.H., Toracinta, E.R., Oglesby, R.J., Fastook, J.L., Hughes, T.J., 2005. LGM summer climate on the southern margin of the Laurentide ice sheet: wet or dry?*. Journal of Climate 18, 3317–3338.
Bronk Ramsey, C., 2008. Deposition models for chronological records. Quaternary Science Reviews 27, 42–60.
Bronk Ramsey, C., 2009. Bayesian analysis of radiocarbon dates. Radiocarbon 51, 337–360.
Caldwell, P., 2010. California wintertime precipitation bias in regional and global climate models. Journal of Applied Meteorology and Climatology 49, 2147–2158.
Cayan, D.R., Mauer, E.P., Dettinger, M.D., Tyree, M., Hayhoe, K., 2008. Climate change scenarios for the California region. Climatic Change 87, S21–S42.
Chávez-Lara, C.M., PRoy, P.D., Perez, L., Muthu Sankar, G., Lemus-Neri, V.H., 2015. Ostracode and C/N based paleoecological record from Santiaguillo Basin of subtropical Mexico over last 27 cal kyr BP. Revista Mexicana de Ciencias Geologicas 32, 1–10.
Cohen, A.S., 2003. Paleolimnology: the History and Evolution of Lake Systems. Oxford University Press, New York.
COHMAP members, 1988. Climatic change of the past 18,000 years: observations and model simulations. Science 241, 1043–1052.
Corbosiero, K.L., Dickinson, M.J., Bosart, L.F., 2009. The contribution of eastern North Pacific tropical cyclones to the rainfall climatology of the southwest United States. Monthly Weather Review 137, 2415–2435.
Deplazes, G., Lückge, A., Peterson, L.C., Timmermann, A., Hamann, Y., Hughen, K.A., Röhl, U., Laj, C., Cane, M.A., Sigman, D.M., Haug, G.H., 2013. Links between tropical rainfall and North Atlantic climate during the last glacial period. Nature Geoscience 6, 213–217.
Douglas, M.W., Maddox, R.A., Howard, K., Reyes, S., 1993. The Mexican Monsoon. Journal of Climate 6, 1665–1677.
Enzel, Y., Wells, S.G., Lancaster, N., 2003. Late Pleistocene lakes along the Mojave river, southwest California. In: Enzel, Y., Wells, S.G., Lancaster, N. (Eds.), Paleoenvironments and Paleohydrology of the Mojave and Southern Great Basin Deserts. Geological Society of America Special Paper 368, pp. 61–77.
Farfán, L.M., Fogel, I., 2007. Influence of tropical cyclones on humidity patterns over southern Baja California, Mexico. Monthly Weather Review 135, 1208–1224.
Flower, B.P., Hastings, D.W., Hill, H.W., Quinn, T.M., 2004. Phasing of deglacial warming and Laurentide icesheet melt water in the Gulf of Mexico. Geology 32, 597–600.
Friedman, I., Smith, G.I., Gleason, J.D., Warden, A., Harris, J.M., 1992. Stable isotope composition of waters in Southeastern California 1. Modern precipitation. Journal of Geophysical Research 97, 5795–5812.
Higgins, R.W., Yao, Y., Wang, X.L., 1997. Influence of the North American Monsoon system on the U.S. summer precipitation regime. Journal of Climate 10, 2600–2622.
Holmgren, C.A., Peñalba, M.C., Rylander, K.A., Betancourt, J.L., 2003. A 16,000 ^{14}C yr B.P. packrat midden series from the USA–Mexico borderlands. Quaternary Research 60, 319–329.
Holmgren, C.A., Norris, J., Betancourt, J.L., 2007. Inferences about winter temperature and summer rains from the late Quaternary record of C_4 perennial grasses and C_3 desert shrubs in the northern Chihuahua Desert. Journal of Quaternary Science 22, 141–161.
Jones, S., Harr, P.A., Abraham, J., Bosart, L.F., Bowyer, P.J., Evans, J.L., Hanley, D.E., Hanstrum, B.N., Hart, R.E., Lalaurette, F., Sinclair, M.R., Smith, R.K., Thorncroft, C., 2003. The extratropical transition of tropical cyclones: forecast challenges, current understanding, and future directions. Weather and Forecasting 18, 1052–1092.
Kim, S.-J., Crowley, T.J., Erickson, D.J., Govindasamy, B., Duffy, P.B., Lee, B.Y., 2008. High-resolution climate simulation of the last glacial maximum. Climate Dynamics 31, 1–16.
Kirby, M.E., Lund, S.P., Poulsen, C.J., 2005. Hydrologic variability and the onset of modern El Niño-Southern Oscillation: a 19250 year record from Lake Elsinore, southern California. Journal of Quaternary Science 20, 239–254.
Kirby, M.E., Lund, S.P., Bird, B.W., 2006. Mid-Wisconsin sediment record from Baldwin Lake reveals hemispheric climate dynamics (Southern CA, USA). Palaeogeography, Palaeoclimatology, Palaeoecology 241, 267–283.
Kirby, M.E., Feakins, S.J., Bonuso, N., Fantozzi, J.M., Hiner, C.A., 2013. Latest Pleistocene to Holocene hydroclimates from Lake elsinore, California. Quaternary Science Reviews 76, 1–15.
Kutzbach, J.E., Wright, H.E., 1985. Simulation of the climate of 18,000 yr B.P.: results for North America/North Atlantic/European Sector. Quaternary Science Reviews 4, 147–187.
Lachniet, M.S., Asmerom, Y., Bernal, J.P., Polyak, V.J., Vazquez-Selem, L., 2013. Orbital pacing and ocean circulation-induced collapses of the Mesoamerican monsoon over the past 22,000 y. Proceedings of the National Academy of Sciences 110, 9255–9260.

Lachniet, M.S., Denniston, R.F., Asmerom, Y., Olyak, V.J., 2014. Orbital control of Western North America atmospheric circulation and climate over two glacial cycles. Nature Communications 5, 3805. http://dx.doi.org/10.1038/ncomms4805.
Lyle, M., Heusser, L., Ravelo, C., Yamamoto, M., Barron, J., Diffenbaugh, N.S., Herbert, T., Andreasen, D., 2012. Out of the Tropics: the Pacific, Great Basin Lakes, and Late Pleistocene water cycle in the western United States. Science 337, 1629–1633.
McClymont, E.L., Ganeshram, R.S., Pichevin, L.E., Talbot, H.M., van Dongen, B.E., Thunell, R.C., Haywood, A.M., Singarayer, J.S., Valdes, P.J., 2012. Sea-surface temperature records of Termination 1 in the Gulf of California: challenges for seasonal and interannual analogues of tropical Pacific climate change. Paleoceanography 27, 1–15, PA2202.
Metcalfe, S.E., Barron, J.A., Davies, S.J., 2015. The Holocene history of the North American Monsoon: 'known knowns' and 'known unknowns' in understanding its spatial and temporal complexity. Quaternary Science Reviews 120, 1–27.
Meyers, P.A., Ishiwatari, R., 1995. Organic matter accumulation records in lake sediments. In: Lerman, A., Imboden, D., Gat, J. (Eds.), Physics and Chemistry of Lakes. Springer-Verlag, New York, pp. 279–328.
Mitchell, D.L., Ivanova, D., Rabin, R., Brown, T.J., Redmond, K., 2002. Gulf of California sea surface temperatures and the North American Monsoon: mechanistic implications from observations. Journal of Climate 15, 2261–2281.
Neelin, J.D., Langenbrunner, B., Meyerson, J.E., Hall, A., Berg, N., 2013. California winter precipitation change under global warming in the coupled model intercomparison project phase 5 ensemble. Journal of Climate 26, 6238–6257.
Nesbitt, H.W., Young, G.M., 1984. Prediction of some weathering trends of plutonic and volcanic rocks based on thermodynamic and kinetic considerations. Geochimica et Cosmochimica Acta 48, 1523–1534.
Nesbitt, H.W., Young, G.M., 1989. Formation and diagenesis of weathering profiles. Journal of Geology 97, 129–147.
NGRIP project members, 2004. High-resolution record of Northern Hemisphere climate extending into the last interglacial period. Nature 431, 147–151.
Nieto-Samaniego, A.F., Barajas-Gea, C.I., Gómez-González, J.M., Rojas, A., Alaniz-Álvarez, S.A., Xu, S., 2012. Geología, evolución structural (Eoceneo al actual) y eventos sísmicos del Graben de Santiaguillo, Durango, México. Revista Mexicana de Ciencias Geológicas 29, 115–130 (In Spanish).
Oster, J.L., Ibarra, D.E., Winnick, M.J., Maher, K., 2015. Sterring of westerly storms over western North America at the Last Glacial Maximum. Nature Geoscience 8, 201–205.
Pettet, D.M., 2009. Younger Dryas. In: Gornitz, V. (Ed.), Encyclopedia of Paleoclimatology and Ancient Environments. Springer, Dordrecht, pp. 993–995.
Reimer, P.J., Bard, E., Bayliss, A., Beck, J.W., Blackwell, P.G., Ramsey, C.B., Grootes, P.M., Guilderson, T.P., Haflidason, H., Hajdas, I., Hatté, C., Heaton, T.J., Hoffmann, D.L., Hogg, A.G., Hughen, K.A., Kaiser, K.F., Kromer, B., Manning, S.W., Niu, M., Reimer, R.W., Richards, D.A., Scott, E.M., Southon, J.R., Staff, R.A., Turney, C.S.M., van der Plicht, J., 2013. IntCal13 and MARINE13 radiocarbon age calibration curves 0–50000 years cal BP. Radiocarbon 55, 1869–1887.
Ritchie, E.A., Elsberry, R.L., 2007. Simulations of the extratropical transition of tropical cyclones: phasing between the upper-level trough and tropical cyclone. Monthly Weather Review 135, 862–876.
Ritchie, E.A., Wood, K.M., Gutzler, D.S., White, S.R., 2011. The influence of eastern Pacific tropical cyclone remnants on the Southwestern United States. Monthly Weather Review 139, 192–210.
Roy, P.D., Caballero, M., Lozano, R., Ortega, B., Lozano, S., Pi, T., Israde, I., Morton, O., 2010. Geochemical record of Late quaternary paleoclimate from lacustrine sediments of paleo-lake San Felipe, western Sonora Desert, Mexico. Journal of South American Earth Sciences 29, 586–596.
Roy, P.D., Jonathan, M.P., Pérez-Cruz, L.L., Sánchez-Córdova, M.M., Quiroz-Jiménez, J.D., Romero, F.M., 2012. A millennial-scale Late Pleistocene–Holocene palaeoclimatic record from the western Chihuahua Desert, Mexico. Boreas 41, 707–717.
Roy, P.D., Quiroz-Jiménez, J.D., Pérez-Cruz, L.L., Lozano-García, S., Metcalfe, S.E., Lozano-Santacruz, R., López-Balbiaux, N., Sánchez-Zavala, J.L., Romero, F.M., 2013. Late Quaternary palaeohydrological conditions in the drylands of northern Mexico: a summer precipitation proxy record of the last 80 ka. Quaternary Science Reviews 78, 342–354.
Roy, P.D., Quiroz-Jiménez, J.D., Chávez-Lara, C.M., Sánchez-Zavala, J.L., Pérez-Cruz, L.L., Muthu Sankar, G., 2014. Humid Pleistocene–Holocene transition and early Holocene at sub-tropical Northern Mexico and possible Gulf of California forcing. Boreas 43, 577–587.
Sanchez Goñi, M.F., Harrison, S.P., 2010. Millennial-scale climate variability and vegetation changes during the Last Glacial: Concepts and terminology. Quaternary Science Reviews 29, 2823–2827.
Sheppard, P.R., Comrie, A.C., Packin, G.D., Angersbach, K., Hughes, M.K., 2002. The climate of the US Southwest. Climate Research 21, 219–238.
Stensrud, D.J., Gall, R.L., Mullen, S.L., Howard, K.W., 1995. Model climatology of the Mexican Monsoon. Journal of Climate 8, 1775–1794.
Talbot, M.R., Johannessen, T., 1992. A high-resolution palaeoclimatic record for the last 27,500 years in tropical West Africa from carbon and nitrogen isotope composition of lacustrine organic matter. Earth and Planetary Science Letters 110, 23–37.
Thompson, R.S., Anderson, K.H., 2000. Biomes of western North America at 18,000, 6,000 and 0 ^{14}C yr BP reconstructed from pollen and packrat midden data. Journal of Biogeography 27, 555–584.
Toracinta, E.R., Oglesby, R.J., Bromwich, D.H., 2004. Atmospheric response to modified CLIMAP ocean boundary conditions during the Last Glacial Maximum. Journal of Climate 17, 504–522.
Wagner, J.D.M., Cole, J.E., Beck, J.W., Patchett, P.J., Henderson, G.M., Barnett, H.R., 2010. Moisture variability in the southwestern United States linked to abrupt glacial climate change. Nature Geoscience 3, 110–113.
Xu, J., Gao, X., Shuttleworth, J., Sorooshian, S., Small, E., 2004. Model climatology of the North American Monsoon onset period during 1980–2001. Journal of Climate 17, 3892–3906.

https://doi.org/10.1016/j.yqres.2015.10.002 Published online by Cambridge University Press